Proceedings of the 6th International Conference on Gas Hydrates (ICGH 2008),
Vancouver, British Columbia, CANADA, July 6-10, 2008.

GEOMECHANICAL RESPONSE OF KNOWN PERMAFROST HYDRATE DEPOSITS TO DEPRESSURIZATION-INDUCED PRODUCTION

Jonny Rutqvist*, George J. Moridis
Earth Sciences Division
Lawrence Berkeley National Laboratory
MS 90-1116, Berkeley, CA, 947 20
USA

Tarun Grover
Petroleum Engineering Department
Texas A&M University
MS 3116, Richardson Building
College Station, TX, 77843
USA

Timothy Collett
U.S. Geological Survey
Denver Federal Center
Box 25046, MS-939
Denver, CO 80225
USA

ABSTRACT

In this simulation study, we analyzed the geomechanical response of two known Class 3 permafrost deposits: the Mallik (Northwest Territories, Canada) deposit and Mount Elbert (Alaska, USA) deposit. Gas was produced from these deposits at constant pressure using horizontal wells placed at the top of the hydrate layer (HL). The depressurization-induced dissociation begins at the well bore, and then spreads laterally mainly along the top of the HL. The depressurization results in an increased shear stress within the body of the receding hydrate, and causes a vertical compaction of the reservoir. However, its effects are partially mitigated by the relatively stiff permafrost overburden, and compaction is limited to less than 0.5%. The increased shear stress may lead to shear failure in the hydrate-free zone that is bounded by the HL overburden and the downward-receding upper dissociation interface. This zone undergoes complete hydrate dissociation, and the cohesive strength of the sediment is low. We determined that the likelihood of shear failure depends on the initial stress state, as well as on the geomechanical properties of the reservoir. The Poisson's ratio of the hydrate-bearing formation is a particularly important parameter that determines whether the evolution of the reservoir stresses will increase or decrease the likelihood of shear failure.

Keywords: gas hydrates, permafrost deposits, depressurization, dissociation, geomechanics

NOMENCLATURE

$k_{h,v}$	Horizontal/vertical permeability [m^2]
E	Young's modulus of elasticity [Pa]
P	Pressure [Pa]
$Q_{R,P}$	Gas production/release rate [ST m^3/s]
S_H	Hydrate saturation
T	Temperature [°C]
U_Z	Displacement [m]
$V_{R,P}$	Released/produced gas volume [ST m^3]
ε_v	Volumetric strain
ε_Z	Vertical compaction
ν	Poisson's ratio
σ_v	vertical stress gradient [Pa/m]
$\sigma_{H,h}$	Horizontal stress gradient [Pa/m]
$\sigma'_{1,3}$	max, min principal stresses [Pa]

* Corresponding author: Phone: +1 510 486 5432 Fax +1 510 486 5686 E-mail: jrutqvist@lbl.gov

INTRODUCTION

Background

Hydrates are solid crystalline compounds in which small gas molecules (referred to as guests) are lodged within the lattices of ice crystals (called hosts). The dominant gas in natural hydrate accumulations is CH_4. These are stable under conditions of low temperature *T* and high pressure *P* in two different geologic settings: in the permafrost and in deep oceans.

The assessment of the global inventory of hydrate distribution in geologic media is in an embryonic state, and the various estimates vary by as much as several orders of magnitude [1]. However, the scientific consensus is that the total amount of CH_4 (and other hydrocarbons) trapped in hydrates is enormous, and easily exceeds the equivalent of all the known conventional oil and gas. The rapidly escalating global energy demand has helped put forth the question of whether hydrates can be developed and exploited as a potential energy source. To address this issue, a significant international research effort has begun recently [2]. Of the three possible methods of hydrate dissociation [3] for gas production (i.e., depressurization, thermal stimulation, and use of inhibitors), depressurization is considered to be the most effective and economically promising method (and probably the only viable alternative) for the commercial production of natural gas from hydrate deposits [4,5,6].

Among the serious technical challenges facing the issue of gas production from hydrates [2], geomechanical considerations are particularly important because they affect the integrity of the formation and the well stability, and can by themselves prevent the exploitation of otherwise promising hydrate accumulations.

Hydrate deposits that are suitable targets for gas production often involve unconsolidated sediments that are usually characterized by limited shear strength. The dissociation of the solid hydrates (a strong cementing agent) during gas production can undermine the structural stability of hydrate-bearing sediments (HBS). This is further exacerbated by the evolution of expanding gas zones, the progressive transfer of loads from the hydrate to the sediments, and subsidence. Additionally, the depressurization of a hydrate deposit may lead to a more anisotropic stress field, potentially leading to shear failure within the dissociating hydrate accumulation. Thus, the potential geomechanical response of hydrate deposits, and their impact on the system flow behavior and resource recovery, need to be carefully evaluated before commercial-scale gas production from permafrost deposits can be developed. This study focuses on this issue.

Objective and approach

The objective of this simulation study is to analyze the geomechanical response of two permafrost Class 3 deposits under production, and to develop the first-ever first assessment of the impact of production on the well stability and the likelihood of formation failure. The state of knowledge on the subject is embryonic at best because the general dearth of information is compounded by the significant geomechanical complication of the "stiff" permafrost overburden. Although the geomechanical response of marine hydrate deposits with compressible overburdens has received some attention in the past [7], to the authors' knowledge, this analysis of permafrost systems is the first study of its kind.

The two hydrate deposits investigated in this study are (a) the Mallik accumulation (Mackenzie Delta, Northwest Territories, Canada) and (b) the Mount Elbert deposit (North Slope, Alaska, USA). Both deposits have been, and still are, the site of past and present studies, from which a large body of information has been acquired. Thus, it is no exaggeration that these two deposits are probably among the best characterized.

The importance of these two deposits, and the reason for their selection for this analysis, stem from the fact that they are likely to be among the sites considered for the design, development and execution of the first large-scale, long-term gas production test [2]. The reasons for their suitability for such a long-term test include [2] (a) the confirmed presence of hydrates at high saturations, (b) occurrence of high-quality hydrate-bearing sediments, (c) site accessibility through proximity to infrastructure, and (d) site knowledge. This being the case, it is imperative to determine as early as possible if there are any geomechanical restrictions (or even barriers) to gas production from such permafrost hydrate deposits, and, should this be the case, to develop strategies to overcome them.

The numerical simulation studies discussed in this paper involve linking the TOUGH+ HYDRATE simulator [4,5,8,9] of hydrate behavior in geologic media with the FLAC3D [10] commercial geomechanical code. The numerical approach, linking process and the operation of the coupled codes have been described in detail by Rutqvist and Moridis [7] and Rutqvist et al. [11] in their analysis of the geomechanical behavior of oceanic HBS.

The investigation approach involves simulation of 5 years of continuous gas production at the two sites using horizontal wells that were kept at a constant bottom-hole pressure P_w = 2.7 MPa, i.e., slightly above the quadruple point in order to prevent the formation of ice in the reservoir. The geomechanical properties of the hydrate bearing sediments and the initial stress field are treated as perturbation parameters in the sensitivity analysis component of the study. This approach is dictated by the lack of site-specific data and uncertainties in the estimation of these parameters at the two sites. During this production period, we monitor the production performance, the evolution of key thermodynamic and geomechanical parameters, and we provide side-by-side comparison of the geomechanical responses at the two sites.

DESCRIPTION OF THE STUDY SITES

The discussion in this section follows closely the analyses of Dallimore et al. [12], Dallimore and Collett [13], Collett [6] and which are the most thorough treatises of the subject.

The Mallik gas hydrate accumulation

The Mallik field is probably the best-characterized gas hydrate accumulation in the world. It is located at the northeastern edge of Canada's Mackenzie Delta, within a sequence of Tertiary sediments in an area underlain by about 600 m of permafrost. Detailed geologic and engineering data on gas hydrates and associated sediments are available [12,13]. Quantitative well-log determinations and core studies reveal at least 10 discrete gas hydrate layers exceeding 110 m in total thickness from approximately 900 to 1,100 m depth. The gas hydrate intervals have high gas hydrate saturation values that, in some cases, exceed 80% of the pore volume [12,13], with the estimates of the amount of trapped gas in the 1 to 10 TCM range [14]. These attributes establish the Mallik field as one of the most concentrated gas hydrate reservoirs in the world.

Recognizing that the Mallik gas hydrate accumulation was an ideal site for a field test of gas production from a natural gas hydrate, an international partnership was formed to carry out a production research program in 2002 [13]. Field operations for the 2002 Mallik program were carried out during the winter of 2001/2002 [13], and provided an extensive data set covering a wide spectrum of subjects related to natural hydrate deposits: geology, geophysics, geochemistry, microbiology, kinetics of gas hydrate dissociation, geomechanics, petrophysical, thermal and hydraulic properties, etc. The production testing included short duration, small-scale pressure drawdown tests and a 5-day thermal stimulation test. The allowed the calibration of several numerical models, the determination of important properties and parameters, and an assessment of the long-term production response of a gas hydrate accumulation [13].

The Mount Elbert gas hydrate accumulation

Studies of pressurized core samples, downhole logs, and production testing at the Northwest Eileen State-2 well (located in the northwest part of the Prudhoe Bay Field) provided the first direct confirmation of gas hydrates on the North Slope (where the Mount Elbert deposit is located) by identifying three hydrate-bearing stratigraphic units [M6]. Based on downhole log data from an additional 50 wells in the same area, Collett [6] identified hydrate units in six laterally continuous sandstone and conglomerate. The volume of gas within this area is estimated at about twice that of the known conventional gas in the Prudhoe Bay Field, ranging between 35 and 42 TCF [6].

A collaborative project that aims to determine the viability of the North Slope hydrates as an energy source is currently in progress [15]. In 2007, a well was installed at an accumulation named the "Mount Elbert" prospect to acquire critical reservoir data needed to develop a longer-term production test program. The well was drilled through 590 m of permafrost to a depth of 915 m, and achieved recovery of significant lengths of core of the hydrate intervals. These were used for subsequent investigations on the pore water geochemistry, microbiology, gas chemistry, petrophysical properties, and thermal and physical properties. A flow test that was conducted in two sandy hydrate-bearing sections with high S_H (60% to 75% yielded gas in both tests. This study has provided one of the most comprehensive datasets yet compiled on a natural hydrate accumulation [6].

Analysis of the data collected from the well will be used to support decisions on the advisability, site selection, well type and location, production method and timing of the next phase of the project. This is currently envisioned as a long-term production test to determine the reservoir deliverability and the gas production potential of permafrost deposits under a variety of well design and operation scenarios.

SIMULATED SYSTEM & APPROACH

Analysis of the geology of the two sites indicates that the hydrate-bearing sediment sequences at both Mallik and Mt. Elbert are mainly composed of sand and weakly cemented sandstones with silt/shale interbeds, confined by nearly impermeable shale boundaries. As such, they are typical representatives of Class 3 deposits [5].

Geometry, boundaries and discretization

The geometry of the rectangular 3D system (stencil) we consider in this study has a square cross section in (x,y) and a side length of 800 m. A horizontal well is placed at the top of the hydrate layer (HL) along the x = 400 m axis. Because of symmetry (a) along the y axis and (b) about the x = 400 m axis, it suffices to simulate a 2D slice in (x,z) that has a unit thickness along the 3rd dimension (ΔY = 1m), includes the entire system profile (from the surface to 30 m below the HL into the underburden) along the z coordinate, and is ΔX = 400 long along the x coordinate (Figure 1 and Table 1). The (x,z) plane of the simulated domain and the location of the horizontal well are clearly shown in the lower part of Figure 1. Because of symmetry, there is no flow of fluids and heat through the lateral boundaries (vertical sides) of the domain. For the same reason, we impose a restriction of zero-displacement normal to these boundary surfaces. The top boundary, representing the ground surface, is kept at constant T and P, but is allowed to move. The bottom boundary (placed at a depth of 30 m below the HL) has a fixed P and T, and a restriction of zero-displacement along the z-axis, i.e., normal to the boundary.

In the case of the Mallik deposit, the 2D domain was discretized in 120x100 = 12,000 elements in (x,z), resulting in 36,000 equations when the equilibrium dissociation option was invoked. The discretization of the 2D domain in the Mt. Elbert cases resulted in 120x93 = 11,160 elements in (x,z) and 34,800 equations. In both cases, discretization along the x-axis is logarithmic (with an initial Δx = 0.1 m), and the vertical discretization is variable. The fine discretization of Δz = 0.25 m in the HL allows an accurate description of the dynamic processes occurring there.

Initial conditions

Table 2 presents the initial conditions at the base of the HL at the two sites. The initial P, T and stresses are higher at the Mallik deposit because of a greater depth. The initial S_H is about 75% at the Mallik deposit, and 65% at the Mt. Elbert accumulation. The initial stress gradients for both sites are based on site geomechanical investigations at the Mallik area [16]. The vertical stress gradient is about σ_v = 19.6 MPa/km corresponding to a bulk density of the overlying permafrost zone of about 2000 kg/m^3. Based on estimates by McLellan et al. [16], the horizontal stresses $\sigma_H = \sigma_h$ in the region range between 13.2 to 18.8 MPa/km, i.e., they are lower than the vertical stresses.

Our approach in this study involves a set of two simulations: (1) the reference (base) case is based on an average horizontal stress gradient of 15 MPa/km (i.e., $\sigma_H = \sigma_h = 0.77\sigma_v$), and (2) the bounding case assumes the lower bound of horizontal stress gradient in the calculations, i.e., $\sigma_H = \sigma_h = 0.67\sigma_v$ = 13.2 MPa/km. This lower σ_H bound corresponds to a geologic medium that is near critically stressed for shear, i.e. with pre-existing fractures and with the unconsolidated sand near its frictional limit. This is consistent with the observed pattern of natural fractures at the Mallik deposit, which indicates that the conjugate shear fractures dip about 60° [17].

Hydraulic and thermal properties

Table 3 presents some of the main input hydrological and thermal properties for Mallik and Mt. Elbert deposits. The hydraulic and thermal properties for the Mallik site are based on the laboratory and field data published in [12,13]. The hydraulic and thermal properties used for the Mt. Elbert study were those used in the code comparison study of Anderson et al. [18]. These include information gleaned from geophysical well logs, as well as flow parameters that were estimated by history-matching the data from a short-term open-hole depressurization test [18]. As can be seen in table 3, the hydraulic and thermal properties are similar at the two sites.

Geomechanical properties

The mechanical properties of the reservoir and overlying rock are of particular importance, but they are also the most uncertain. Some information on the geomechanical properties at the Mallik site can be deduced from geophysical surveys conducted during past research activities [13, 17, 19]. For example, Figure 2 presents vertical profiles of compressional- and shear-wave

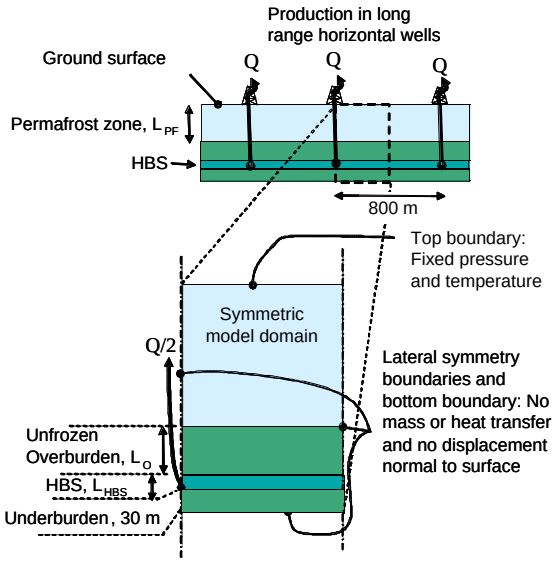

Figure 1: Simulation domain geometry.

Dimensions	Mallik	Mt. Elbert
Permafrost zone, L_{PF} (m)	606	590
Unfrozen overburden thickness, L_o (m)	300	60
HL depth (m)	906 to 930	650 to 661.25
HL thickness, L_{HBS} (m)	11.25	24
Underburden thickness (m)	30	30
Well spacing (m)	800	800

Table 1. Model dimensions for Mallik and Mt. Elbert (see Figure 1).

Parameter	Mallik	Mt. Elbert
Pressure (MPa)	≈ 9.1	≈ 6.6
Temperature (ºC)	≈ 7.2	≈ 2.8
Hydrate saturation (%)	75	65
Vertical stress (MPa)	17.6	12.7
Horizontal stress (MPa)	13.6	9.7

Table 2. Initial conditions at the base of the HL in the Mallik and Mt. Elbert deposits.

Property	Mallik	Mt. Elbert
Permeability (mD)	k_h = 1200 k_h/k_v = 10	k_h = 1000 k_h/k_v = 10
Porosity (%)	37	35
Grain density (kg/m^3)	2650	2650
Wet thermal conductivity (W/m/K)	2.24	3.1
Dry thermal conductivity (W/m/K)	1	1
Grain Specific Heat (J/kg/K)	1000	1000

Table 3. Hydrological and thermal properties for Mallik and Mt. Elbert.

velocity from Vertical Seismic Profiling and sonic logs at Mallik [19]. The sonic velocities are functions of dynamic elastic properties and can be used to estimate the magnitude of, and variability in, the static elastic and strength properties [20]. Using compressional and shear-wave velocity logs from the Mallik 5L-38 well and Gaussmann's [21] equations, estimates of the dynamic elastic properties have been obtained [13]. The Mallik 5L-38 sonic log data show that compressional-wave velocity increases from about 2000 m/s to about 2500 m/s when transitioning from pure sand to the HL, whereas the shear-wave velocity increases from 1000 to 1500 m/s. The resulting dynamic Poisson's ratio is about 0.4 both inside and outside the HL. The Young's modulus *E* is about 5 GPa outside the HL, and increases to about 15 GPa within the HL. However, values of static, rather than dynamic, properties are needed in a coupled reservoir-geomechanical analysis of stress and strain changes induced by hydrate dissociation.

The results of Winters et al. [22,23] and Uchida et al. [24] from a few laboratory experiments on samples from the Mallik site may be used to estimate the static strength and elastic properties. As expected, the values of the geomechanical properties that are deduced from these laboratory experiments are up to several orders of magnitude lower than those obtained from the sonic well logs at Mallik. On the other hand, the strength and stiffness values of the Mallik samples [22,23,24] are similar to those of Toyoura Sand estimated from laboratory studies [18], and which have used by Rutqvist and Moridis [7] and Rutqvist et al. [11] to study the geomechanical behavior of oceanic hydrate bearing sediments undergoing dissociation.

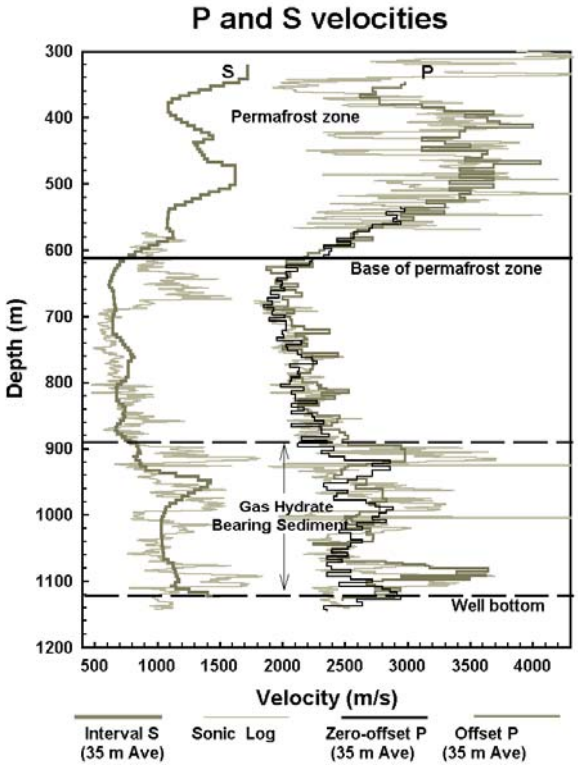

Figure 2: Vertical profiles of compressional- and shear-wave velocity derived from VSP and sonic log analysis at the Mallik well 2L-38 [19].

Adopting these properties implies that the static modulus is about 1/10 of the dynamic one, and that the static Poisson's ration is significantly lower than the sonic one. A reasonable value of Poisson's ratio for sand or weakly cemented sandstone should be less then about 0.25, averaging around 0.15 [20]. The Poisson's ration determined from static laboratory tests on Toyoura Sand ranged from 0.1 to 0.2, and averaged 0.15 independently of the hydrate saturation [25].

For the aforementioned reasons, in our computations we adopted the two sets (static and sonic) of geomechanical properties listed in Table 4. The static properties were based on the experimental data on Toyoura sand [25], and are consistent with the limited laboratory data from Mallik. The sonic properties were estimated from compressional- and shear-wave velocity logs using geophysical standard theory and empirical equations (e.g. [20]). We used the same mechanical properties for the Mallik and Mt. Elbert cases, which is a reasonable approach given the relative similarities of the geological settings of these sites. In the reference case we use the mechanical properties derived from the laboratory experiments on Toyoura Sand [25], which, to the author's knowledge, represent the most complete, systematic and relevant data set on the static mechanical properties of a hydrate-bearing sand. These properties are reasonable, considering the known differences between dynamic and static mechanical properties, and are consistent with the results from the few static geomechanical experiments conducted on samples from the Mallik deposit. For comparison, we run an additional simulation using the dynamic properties to show the importance of complementing sonic log data with systematic laboratory testing.

SIMULATION RESULTS

Because the HL is hydraulically confined by shales, depressurization is rapid and effective, leading to fast hydrate dissociation and considerable cooling during the 5 years of production considered in this study. The constant P_w at the well and the low effective permeability of the HBS creates a pressure disturbance that is characterized by a sharp front coinciding with the dissociation front. This front moves rapidly outward from the well, and it extends laterally along the x-axis after first reaching the bottom of the HL. Because depressurization is localized (being confined to the limited volume of dissociated or rapidly dissociating medium between the well and the front), most mechanical deformations and stress changes reach maximum levels very early, i.e., within the first year of production.

Property	Static Properties	Sonic properties	Property
Cohesion C_m (MPa)	$S_H = 0$	0.5	5
	$S_H = 1$	2.0	20
Friction angle (°)	$S_H = 0$	30	30
	$S_H = 1$	30	30
Young's Modulus E (GPa)	$S_H = 0$	0.5	5
	$S_H = 1$	1.8	18
Poisson's ratio ν	$S_H = 0$	0.15	0.4
	$S_H = 1$	0.15	0.4

Table 4. Two sets (static and sonic) of input geomechanical properties used in the study of the Mallik and Mt. Elbert deposits.

Thus, instead of gradual geomechanical changes that occur over a large reservoir volume, production from hydrates is uniquely characterized by maximum changes that are arrived at early (and then remain practically unchanged) within a small volume that is centered around the well and expands slowly.

Production Performance

Figure 3 shows the evolution of (a) the volumetric rate Q_R of release of the hydrate-originating CH_4 into the reservoir, and (b) the volumetric rate Q_P of CH_4 production, both summed over the entire 800 m length of the horizontal well. The Q_R and Q_P patterns are quite similar (as expected, being both Class 3 deposits in similar geologic settings and with similar properties), and they are both consistent with the behavior of such deposits [5], i.e., with Q_P only slightly lower than Q_R. The Mt. Elbert deposit is slower to respond because of its lower temperature (Table 2), and is considerably less productive than the Mallik deposit. Thus, at t = 5 years, Q_P = 0.7 ST m^3/s (= 2.15 MMSCFD) at the Mallik deposit, but Q_P = 0.11 ST m^3/s (= 0.34 MMSCFD) at Mt. Elbert.

The superiority of the Mallik deposit as a production target is confirmed by the cumulative volumes of released (V_R) and produced (V_P) gas in Figure 4, which show the total Mallik production $V_P = 9 \times 10^7$ ST m^3 (= 3.2 BCF) dwarfing the V_P = 1.53 ST m^3 (= 0.54 BCF) from Mt. Elbert. In addition to its higher temperature, another reason for the superior performance of the Mallik formation is the larger HL thickness

(Table 2). Figure 4 shows very small volumes of free gas in the reservoir, as is typical in production from Class 3 deposits [5].

Figure 3 shows that Q_R and Q_P increase initially rapidly, and then they begin oscillating around a plateau. An increasing trend is observed in the Q_R and Q_P of the Mallik deposit, though not in the Mt. Elbert one. It is not possible to know if these trends will persist later because only a small fraction of the total mass is destroyed at the end of the 5-year production period (Figure 5).

Evolution of thermodynamic state

Figures 6 and 7 show the spatial distributions of P, T, and S_H at t = 3 yrs in the Mallik and Mt. Elbert deposits, respectively. Despite the diffusive nature of P (which is transmitted even when flow is inhibited), a sharp front is easily detected in both figures at a location that roughly matches that of the dissociation front, and is confirmed by the corresponding minimum T (because of the endothermic dissociation reaction) at the same location. Note that dissociation occurs mainly at the top of the HL, but the HL bottom is also beginning to show faint signs of dissociation. Because of reduced dissociation in the colder Mt. Elbert deposit, the edge of the dissociation front reaches only 120 m from the well at t = 3 yrs, compared to 280 m in the Mt. Elbert deposit.

Figure 8 shows the temporal evolution of P, T, and S_H at the top of the HL and at x = 10 m from the production well. Note that (a) the hydrate is destroyed within a short time (10 days in the Mallik deposit, 30 days in the Mt. Elbert one), and (b) after the hydrate exhaustion, P (which controls the geomechanical behavior) remains practically constant. This supports the earlier discussion that geomechanical changes reach their maximum level early.

Evolution of the geomechanical regime

The main geomechanical responses are associated with the depressurization of the hydrate deposit that causes an increase in vertical effective stress, which, in turn, results in increased shear stress and vertical compaction of the reservoir.

Figure 9 shows the evolution of effective principal stresses for the base case, i.e. with static reservoir properties and an initial horizontal stress gradient of 15 MPa/km (i.e., $\sigma_H = \sigma_h = 0.77\sigma_v$). The figure shows that the effective principal stresses in the reservoir change quickly proportionally to the fluid P responses shown in Figure 8. Overall, production (and the corresponding depressurization) tends to increase the shear stress in the reservoir, which is proportional to the difference between the maximum and minimum principal stresses.

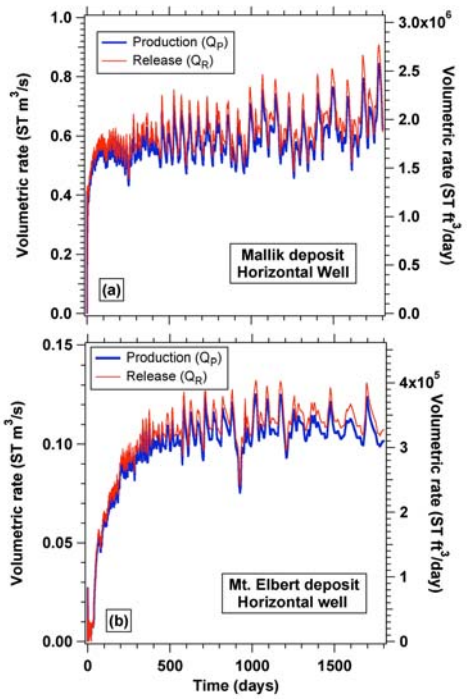

Figure 3: Gas release and production rates from the (a) Mallik and (b) Mt. Elbert deposits.

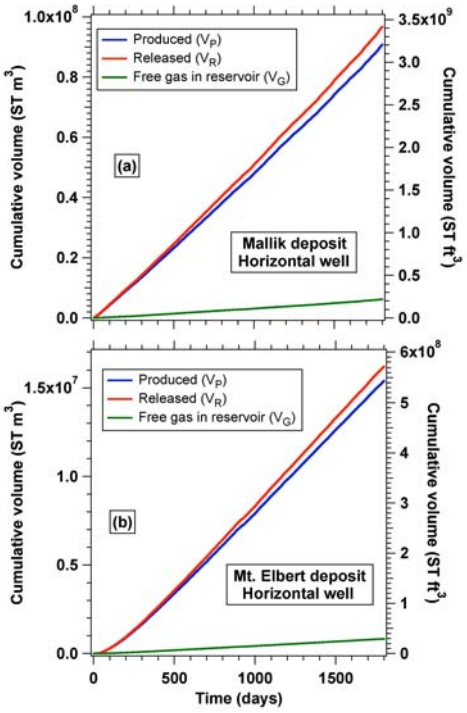

Figure 4: Cumulative volumes of released, produced and free gas in the (a) Mallik and (b) Mt. Elbert deposits.

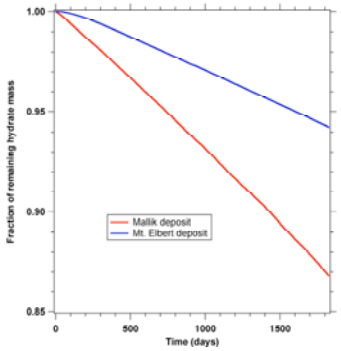

Figure 5: Remaining hydrate in the deposits.

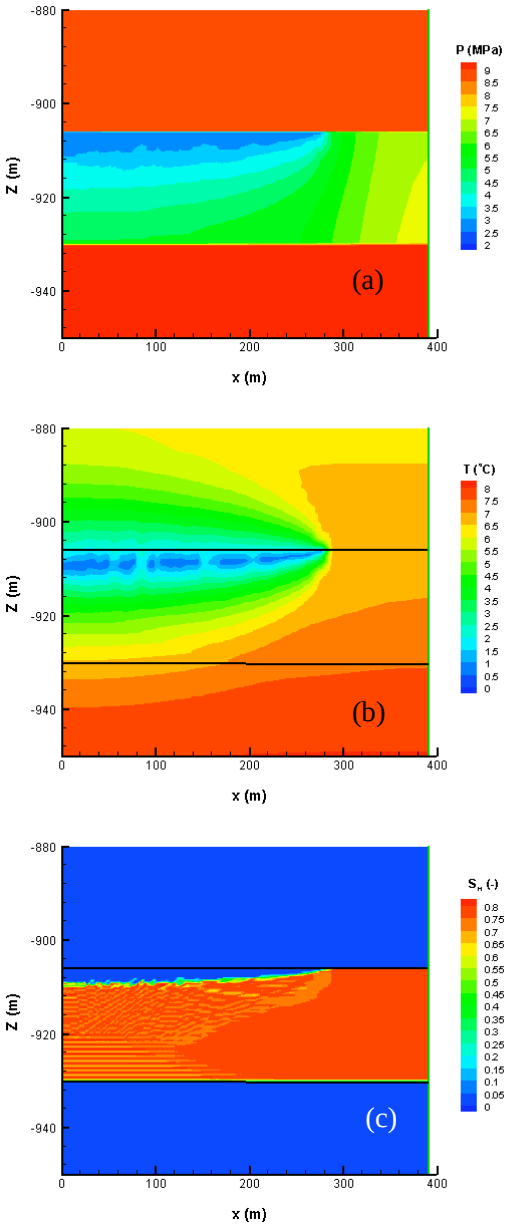

Figure 6: P, T, and S_H distributions at $t = 3$ yrs in the Mallik deposit.

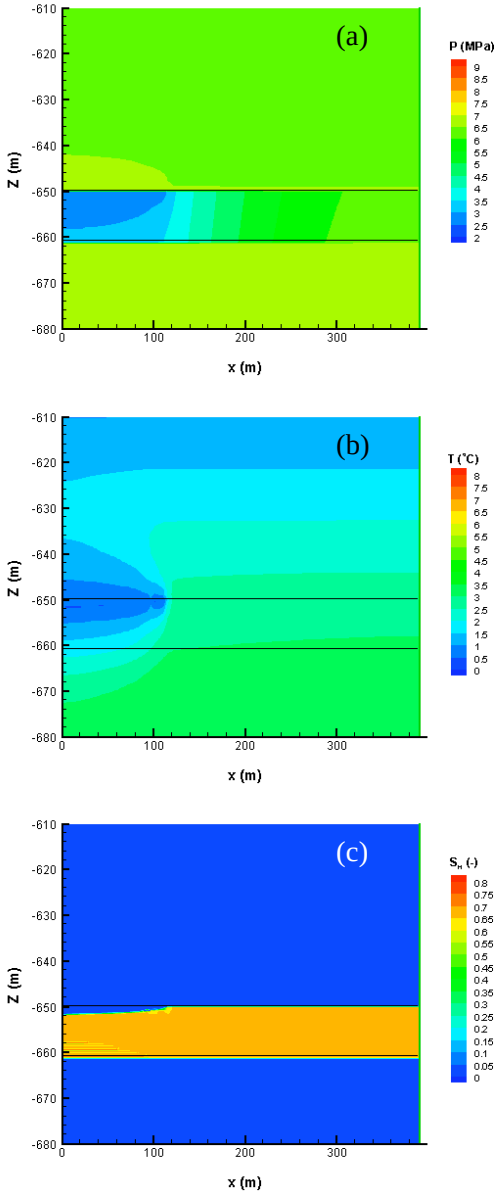

Figure 7: P, T, and S_H distributions at $t = 3$ yrs in the Mt. Elbert and deposit.

The total maximum principal stress σ_1 is approximately constant throughout the simulation, as determined by the weight the overburden rock. The intermediate and minimum compressive principal stresses σ_2 and σ_3 are horizontal and change as a result of poroelastic stressing during depressurization. Figure 10 presents the path of the maximum and minimum principal effective stresses for three different mechanical conditions. The figure shows that the effective principal stress state moves into failure (shaded area) only in the case of static mechanical properties and a low initial horizontal stress (i.e. an initial horizontal stress gradient of 13.2 MPa/km, and

$\sigma_H = \sigma_h = 0.67\sigma_v$). If the initial horizontal stress is higher, the initial effective stress state is much further away from failure and never moves into failure during depressurization. The figure shows that for static properties the stress state moves along a slope $\Delta\sigma'_1/\Delta\sigma'_3 \approx 5.5$, whereas for sonic properties, the stress state moves along an initial slope of $\Delta\sigma'_1/\Delta\sigma'_3 \approx 1.5$. Using the assumption of a thin and laterally extensive reservoir, it can be shown that the slope $\Delta\sigma'_1/\Delta\sigma'_3$ can determined from the Poisson's ratio. For the static Poisson's ratio, $\nu = 0.15$ the slope can be calculated analytically as $\Delta\sigma'_1/\Delta\sigma'_3 = 5.5$ whereas for the sonic Poisson's ratio $\nu = 0.4$ the slope is $\Delta\sigma'_1/\Delta\sigma'_3 = 1.5$. In the numerical simulation result shown in Figure 10, the stress path does not follow exactly these slopes, because the numerical results are affected by changes in elastic properties due to hydrate dissociation, and by thermal stresses. However, the results show that the Poisson's ratio of the reservoir rock is an important parameter that determines whether reservoir stresses during depressurization will increase or decrease the likelihood of shear failure.

Figure 11 present the evolution of the maximum compressive effective stress and strength at the same monitoring point located about 10 m from the production well. At both Mallik and Mt. Elbert deposits, the initial (pre-production) maximum stress is much less than the compressive strength. For example, at Mallik the initial compressive strength is 14.5 MPa for a hydrate saturation of 75%, whereas the maximum compressive effective stress is about 9 MPa. During the depressurization the maximum compressive strength remain much larger than the stress until the hydrate starts to dissociate. At the Mallik, the dissociation and weakening of the sediment implies that failure starts at about 10 days and thereafter the maximum compressive effective stress that the sediment can sustain is limited by the strength of the sediment. At Mt. Elbert, the dissociation is slower due to a smaller depressurization at that site, but shear failure is triggered after about 2 months.

Figure 12 presents the time evolution of the vertical settlement at the ground surface and at the top of the reservoir and the resulting average vertical compaction strain ε_Z. For both the Mallik and Mt. Elbert deposits, ε_Z is restricted by the relatively stiff permafrost overburden. As a result, the vertical settlement U_Z of the ground surface is somewhat smaller then corresponding U_Z at the reservoir, especially at early times. The stiffening effect of the permafrost overburden diminishes as the depressurization of the deposit

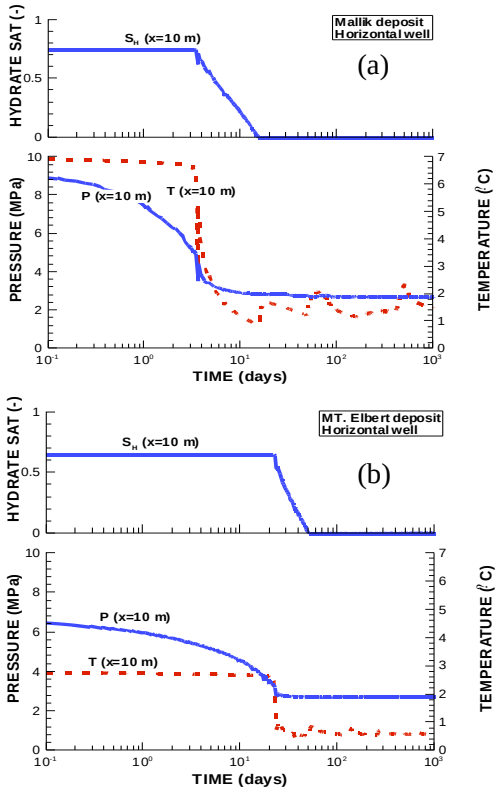

Figure 8. Evolution of S_H, P, and T at the top of the HL of the two deposits at $x = 10$ m.

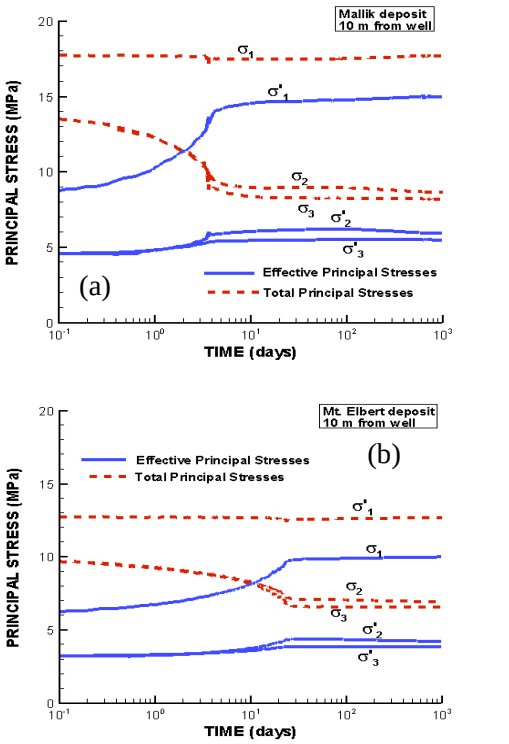

Figure 9. Principal stresses (effective and total) at the top of the HL of the two deposits at $x = 10$ m.

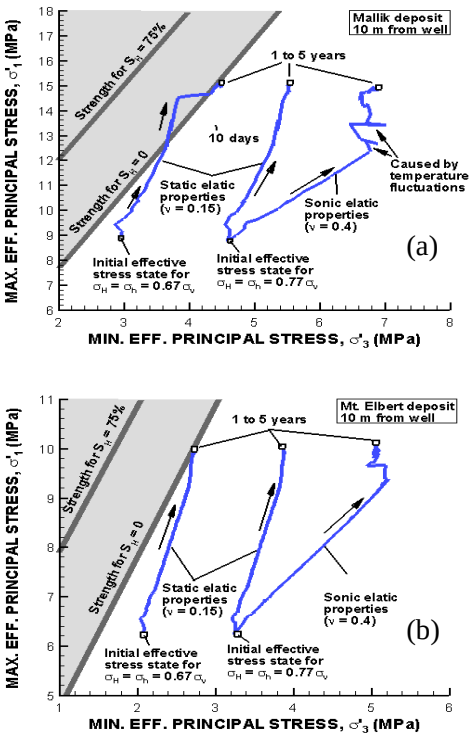

Figure 10: Path of reservoir stress state (σ'_1 vs. σ'_3) for 3 different cases of mechanical parameters at the (a) Mallik and (b) Mt. Elbert deposits.

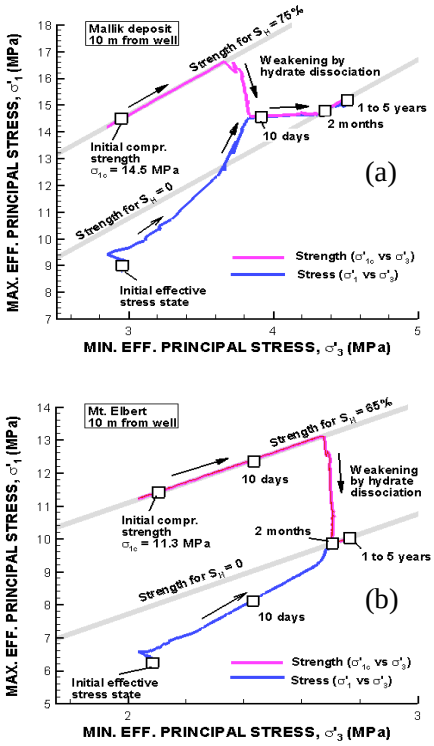

Figure 11: Path of reservoir stress state (σ'_1 vs. σ'_3) and compressive strength (σ'_{1c} vs. σ'_3) at a points at the HL top and x = 10 m.

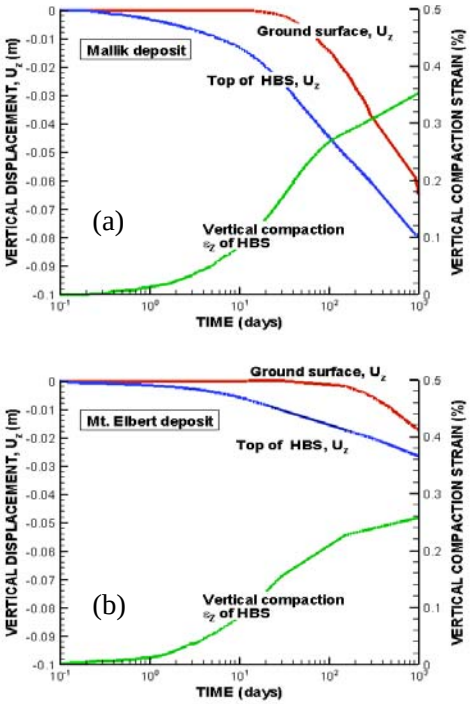

Figure 12. Evolution of U_Z at the ground surface and at the HL top, and of the HBS ε_Z at the (a) Mallik and (b) Mt. Elbert deposits.

becomes more extensive after several years of production. Overall, for the adopted mechanical properties, ε_Z < 0.4% and U_Z = 6 cm at Mallik. The corresponding ε_Z and U_Z are smaller at Mt. Elbert as a result of a smaller depressurization and a thinner deposit. Figure 13 and 14 shows the distribution of volumetric strain ε_V after 1 and 3 years of production. The largest volumetric strain develops within the dissociated zone at the top of the HL. Thus, in this zone there is a more substantial compaction as a result of sediment softening.

CONCLUSIONS AND DISCUSSION

In our study of depressurization-induced gas production from the Mallik and Mt. Elbert Class 3 hydrate deposits using horizontal wells at the HL top that are kept at a constant bottomhole pressure, we reach the following conclusions:

(1) The depressurization causes preferential hydrate dissociation that proceeds mainly along the HL top.

(2) The depressurization of the hydrate reservoir results in vertical compaction of the reservoir and in increased shear stress within the reservoir. The magnitude of vertical compaction and shear stress depends on the magnitude of depressurization and the elastic properties of the reservoir and overlying formations.

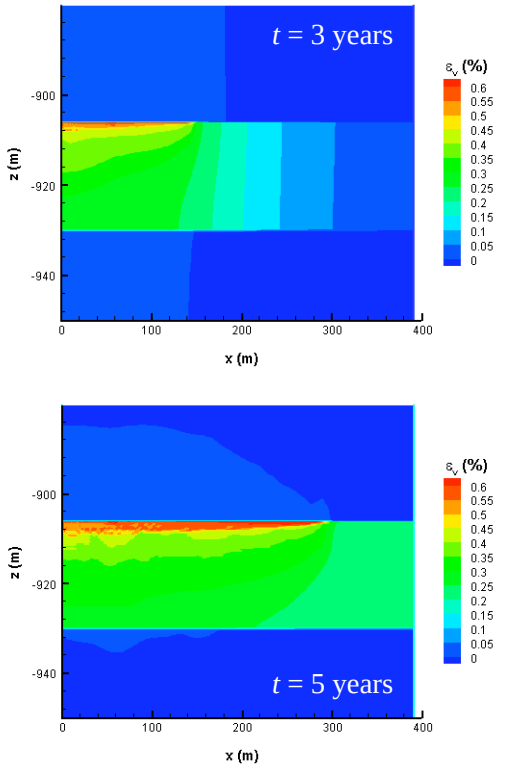

Figure 13: Distribution of ε_V in the Mallik deposit

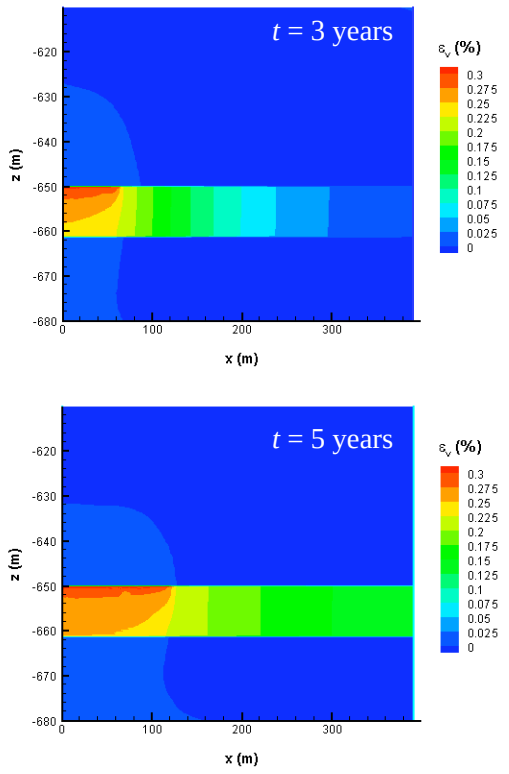

Figure 14: Distribution of ε_V in the Mt. Elbert deposit

(3) The calculated ε_Z is within 0.4%, and the estimated $U_Z < 6$ cm. Of the two deposits, Mallik has the largest ε_Z and U_Z because of larger depressurization and a thicker HL.
(4) Depressurization increases the effective shear stress because the vertical effective stress increases much more then the horizontal effective stress. At both Mallik and Mt. Elbert, the higher shear stress may lead to shear failure in the zone of hydrate dissociation between the HL overburden and the downward-receding upper dissociation interface.
(5) The likelihood of shear failure is strongly dependent on the initial stress state and on the elastic properties of the reservoir. In particular, the Poisson's ratio ν of the HBS is an important parameter determining the effective stress path during depressurization. When a dynamic $\nu = 0.4$ (from sonic logs) is used, the predicted effective stress state always diverges from shear failure during depressurization. When a static $\nu = 0.15$ (a reasonable estimate for unconsolidated sand) is used, the effective stress state will tend towards shear failure, but may not reach it depending on the initial stress state.

This study shows the importance of determining the relationship between static and dynamic properties of HBS. In particular, more laboratory data are needed to constrain static elastic properties (E and ν) as well as strength properties (e.g., cohesion and coefficient of friction) and how these properties vary with S_H. The consequences of shear failure near the top of the reservoir may not all be negative. The shear with associated dilation may increase the permeability, thus enhancing gas production. The increased reservoir shear stress may lead to shear reactivation of pre-existing fractures that may open up, further increasing production. The potential benefits of such shear-enhanced permeability will be subject of future studies.

ACKNOWLEDGMENTS

This work was supported by the Assistant Secretary for Fossil Energy, Office of Natural Gas and Petroleum Technology, through the National Energy Technology Laboratory, under the U.S. Department of Energy Contract No. DE-AC02-05CH11231.

REFERENCES

[1] Sloan ED, Koh C. *Clathrate Hydrates of Natural Gases*. 3rd Edition, Boca Raton, FL: Taylor and Francis, Inc., 2008.
[2] Moridis GJ, Collett TS, Boswell R, Kurihara M, Reagan MT, Koh C, Sloan ED. *Toward Production From Gas Hydrates: Current Status, Assessment of Resources, and Simulation-Based Evaluation of Technology and Potential*. SPE

114163, 2008 SPE Unconventional Reservoirs Conference, Keystone, Colorado, U.S.A., 10–12 February 2008.
[3] Makogon YF. *Hydrates of Hydrocarbons*. Tulsa, OK: Penn Well Publishing Co., 1997.
[4] Moridis GJ, Reagan MT. *Gas Production From Oceanic Class 2 Hydrate Accumulations*, OTC 18866, 2007 Offshore Technology Conference, Houston, Texas, U.S.A., 30 April–3 May 2007.
[5] Moridis GJ, Reagan, MT. *Strategies for Gas Production From Oceanic Class 3 Hydrate Accumulations*, OTC 18865, 2007 Offshore Technology Conference, Houston, Texas, 30 April – 3 May 2007.
[6] Collett TS. *Artic gas hydrate energy assessment studies.* The Artic Energy Summit. Anchorage, Alaska, 2007-2008.
[7] Rutqvist J, Moridis GJ. *Numerical studies on the geomechanical stability of hydrate-bearing sediments*. Offshore Technology Conference, Houston, Texas, USA, April 30-May3, 2008.
[8] Moridis GJ, Kowalsky MB, Pruess K. *Depressurization-Induced Gas Production From Class 1 Hydrate Deposits*, SPE REE 2005: 10(5): 458-481.
[9] Moridis GJ, Kowalsky M, Pruess K. *TOUGH+HYDRATE v 1.0 User's manual,* Report LBNL-149E, Berkeley, CA: Lawrence Berkeley National Laboratory – Earth Sciences Division, 2008.
[10] Itasca Consulting Group. *FLAC3D: Fast Lagrangian Analysis of Continua in 3 dimensions,* Minneapolis, Minnesota. 2002
[11] Rutqvist J, Grover T, Moridis GJ. *Coupled hydrological, thermal and geomechanical analysis of wellbore stability in hydrate-bearing sediments*. Offshore Technology Conference. Houston, Texas,USA, May 5-8, 2008.
[12] Dallimore SR, Uchida T, Collett TS. Editors. *Scientific Results from the JAPEX/JNOC/GSC Mallik 2L-38 Gas Hydrate Research Well, Mackenzie Delta, Northwest Territories, Canada.* Geological Survey of Canada Bulletin 544: 1999.
[13] Dallimore SR, Collett TS, edts. *Scientific Results from the Mallik 2002 Gas Hydrate Production Research Well Program, Mackenzie Delta, Northwest Territories, Canada.* Geological Survey of Canada, Bulletin 585: 2005.
[14] Osadetz KG, Chen Z. *A re-examination of Beaufort Sea – Mackenzie Delta Basin gas hydrate resource potential using a petroleum system approach*: Proceedings of the Fifth International Conference on Gas Hydrates, Trondheim, Norway, June 13-16, 2005.
[15] Mount Elbert Science Team. *Alaska North Slope Well Successfully Cores, Logs, and Tests Gas-Hydrate-Bearing Reservoirs, Fire In The Ice, NETL Methane Hydrates R&D Program Newsletter, Winter 2007.* *(http://www.netl.doe.gov/technologies/oil-gas/publications/ Hydrates/Newsletter/ HMNewsWinter07.pdf).*
[16] McLellan PJ, Gillen KP, Podetz CG, Dallimore SR, Inoue T, Hancock SH. *In situ stresses in the Mallik area.* In: Dallimore SR, Collett TS, editors. Scientific Results from the Mallik 2002 Gas Hydrate Production Research Well Program, Mackenzie Delta, Northwest Territories, Canada. Geological Survey of Canada, Bulletin 585: 2005.
[17] McLellan PJ, Gillen KP, Podetz CG, Dallimore SR. *Characteristics of natural fractures in the JAPEX/JNOC/GCS et al. Mallik 5L-38 gas hydrate production research well.* In: Geological Survey of Canada, Bulletin 585: 2005.
[18] Anderson et al. (12 co-authors). *Analysis of Modular Dynamic Formation Test Results from the "Mount Elbert" Stratigraphic Test Well, Milne Point, Alaska. In: Proceedings of the 6th International Conference on Gas Hydrates (ICGH 2008), Vancouver, British Columbia, Canada, July 6-10, 2008.*
[19] Mi Y, Sakai A, Walia R, Hyndman RD, Dallimore SR. *Vertical seismic profiling and seismic properties of gas hydrate in an Artic well.* CREWES Project Research Report, volume 11, Calgary, Alberta, Department of Geology and Geophysics, Univ. of Calgary, Calgary, 1999.
[20] Zoback M. *Reservoir Geomechanics*: Cambridge University Press., 2007.
[21] Gaussmann , F. Uber die elastizitat poroser medien. (Elasticity of porous media). Vierteljahrsschrift der Naturforschenden Gesselschaft in Zurich, 1951, 96: 1-23.
[22] Winters WJ, Dallimore SR, Collett TS, Katsube TJ, Jenner KA, Cranston RE, Wright JF, Nixon FM, Uchida T. *Physical properties of sediments for the JAPEX/JNOC/GSC. Mallik 2L-38 gas hydrate research well.* Geological Survey of Canada, Bulletin, Rep. 544: 1999.
[23] Winters WJ, Waite WF, Mason DH. *Methane gas hydrate effect on sediment acoustic and strength properties.* Journal of Petroleum Science and Engineering. 2007: 56(1-3): 127-135.
[24] Uchida T, Uchida T, Kato A, Sasaki H, Kono F, Takeya S. *Physical properties of natural gas hydrate and associated gas-hydrate-bearing sediments in the JAPEX/JNOC/GSC et al. Mallik 5L-38 gas hydrate production research well.* In: Geological Survey of Canada, Bulletin 585: 2005.
[25] Masui A, Haneda H, Ogata Y, Aoki K. *The effect of saturation degree of methane hydrate on the shear strength of synthetic methane hydrate sediments. In: Proceedings of the 5th International Conference on Gas Hydrates (ICGH 2005), Trondheim, Norway, June 12-16, 2005.*